JCTC Journal of Chemical Theory and Computation

Article

pubs.acs.org/JCTC

Benchmark Assessment of Density Functional Methods on Group II–VI MX (M = Zn, Cd; X = S, Se, Te) Quantum Dots

Jon M. Azpiroz, Jesus M. Ugalde, and Ivan Infante*

Kimika Fakultatea, Euskal Herriko Unibertsitatea (UPV/EHU) and Donostia International Physics Center (DIPC), P. K. 20080 Donostia, Euskadi, Spain

Supporting Information

ABSTRACT: In this work, we build a benchmark data set of geometrical parameters, vibrational normal modes, and low-lying excitation energies for MX quantum dots, with M = Cd, Zn, and X = S, Se, Te. The reference database has been constructed by *ab initio* resolution-of-identity second-order approximate coupled cluster RI-CC2/def2-TZVPP calculations on $(MX)_6$ model molecules in the wurtzite structure. We have tested 26 exchange-correlation density functionals, ranging from local generalized gradient approximation (GGA) and hybrid GGA to meta-GGA, meta-hybrid, and long-range corrected. The best overall functional is the hybrid PBE0 that outperforms all other functionals, especially for excited state energies, which are of particular relevance for the systems studied here. Among the DFT methodologies with no Hartree–Fock exchange, the M06-L is the best one. Local GGA functionals usually provide satisfactory results for geometrical structures and vibrational frequencies but perform rather poorly for excitation energies. Regarding the CdSe cluster, we also present a test of several basis sets that include relativistic effects via effective core potentials (ECPs) or via the ZORA approximation. The best basis sets in terms of computational efficiency and accuracy are the SBKJC and def2-SV(P). The LANL2DZ basis set, commonly employed nowadays on these types of nanoclusters, performs very disappointingly. Finally, we also provide some suggestions on how to perform calculations on larger systems keeping a balance between computational load and accuracy.

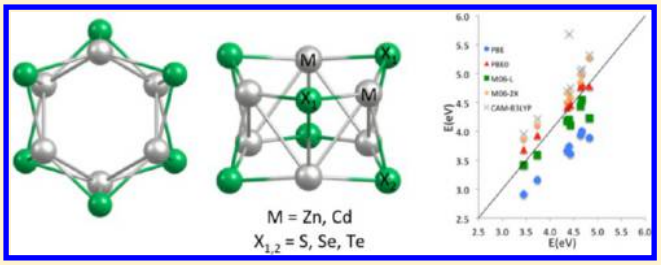

1. INTRODUCTION

Semiconductor quantum dots (QD)[1] have earned lots of attention in recent years for their application in a wide variety of fields[2] including, among others, photovoltaics,[3−7] photocatalysis,[8−11] optical sensing,[12,13] optoelectronics,[14] biotechnology, and medicine.[15,16] Their unique behavior stems from a few main properties: (a) an easily tunable bandgap with the size of the cluster, (b) a high optical extinction coefficient dependent on the large cross sections of these materials, (c) a sharp emission spectrum, (d) the ability to generate more than one photoexcited electron through the phenomenon of carrier multiplication, and (e) a much longer photostability compared to organic photosensible compounds.[17−21]

Despite the great advancements achieved with these nanomaterials, there are still many open questions to be answered. Charge transfer processes involved in the conversion of solar energy into electricity, for example, from a photoexcited QD injecting electrons into a metal oxide semiconductor nanomaterial such as TiO_2, still need to be completely understood.[7] The role of organic ligands attached on the nanocrystal surface or the type of absorption that can occur between the QD and the metal oxide surface, or the effect of trap states induced, for example, by doping the QD or by an incomplete passivation of the reconstructed surface, are still to be fully elucidated.[22] To enable significant advances in the design of novel more efficient materials, theoretical modeling can deliver a formidable help as it allows for accurate simulations of spectroscopic and structural properties of the complex heterocomposite interfaces constituting the QD surface and its interaction with the environment.

Theoretical methodologies that can be utilized to study these systems vary a lot depending on the accuracy that one wants to achieve and the type of properties to be investigated. Usually, the typical size of these nanocrystals, about 2−5 nm, would allow the application of just semiempirical or tight-binding methods, which provide only a limited level of accuracy. However, the advent of density functional theory (DFT) and the possibility to reduce the QD size by means of tailored model systems, smaller and more practical, make these compounds much more affordable from a computational standpoint while keeping in any case a satisfactory level of accuracy. The DFT approximations for the exchange-correlation functional currently available fail to describe the strongly correlated regime, as that found in the two-dimensional electrostatic QDs.[23] In this sense, new methods are being developed, such as the symmetry breaking/restoration methods[24] and modified Kohn–Sham approaches.[25] However, for the QD models considered here, standard DFT methodologies already provide reliable results.

Received: June 17, 2013
Published: December 6, 2013

Table 1. List of Theoretical Papers on II−VI Quantum Dots Sorted by Exchange-Correlation Functionals and Basis Sets[a]

functional		#	refs	basis set				#	refs
LDA	SVWN	10	26, 38−46	localized	numerical		DNP	7	47−53
GGA	PBE	15	27, 39, 51, 54−65		analytical	STO	DZ	3	56, 58, 65, 66
	PW91PW91	11	27, 46−49, 66−71				TZ2P	1	59
	BLYP	3	50, 52, 53			GTO	STO-3G(*)	1	26
	BP86	2	72, 73				DZ(D)P	2	74, 75
	OPBE	1	26				SDD(*)	2	26, 76
HGGA	B3LYP	28	26, 27, 46, 47, 56−58, 65, 72, 74−92				LANL2DZ(*)	16	26, 27, 46, 60, 78, 82−92
	mPW1PW91	2	93, 94				LANL2MB	1	26
	PBE0	2	27, 60				SBKJC(*)	6	47, 65, 77, 80, 93, 94
	BHLYP	1	57				def2-SVP	4	56, 58, 72, 74
MGGA	TPSS	1	27				def2-TZVP	6	27, 57, 73−75, 79
LRC	CAM-B3LYP	1	27				def2-QZVP	1	57
	LC-wPBE	1	27				aug-cc-pVTZ	1	57
				PWs				16	27, 38, 39, 42, 43, 45, 46, 61, 63, 64, 67−71, 95

[a]References are also included. # stands for number of articles. STO = Slater-type orbitals. GTO = Gaussian-type orbitals. PW = plane waves.

Table 2. List of DFT Functionals and Basis Sets Included in This Work and References Therein

type	functional	HF X (%)	refs	basis set	type core	refs
GGA	BLYP		96, 97	LANL2DZ	ECP	98−100
	BP86		96, 101	SBKJC	ECP	102−104
	BPW91		96, 105	def2-SV(P)	ECP	106, 107
	G96LYP		108, 109	def2-TZVPP	ECP	106, 107
	mPWLYP		110	DZ	frozen core (large)	111
	OLYP		112, 113	DZ	frozen core (small)	111
	PBE		114	DZ	all-electron/ZORA	111
HGGA	B1LYP	25	115	TZ2P	all-electron/ZORA	111
	B3LYP	20	116			
	B97-2	21	117			
	mPW1PW91	25	110			
	O3LYP	11.61	118			
	PBE0	25	119			
	X3LYP	21.8	120			
MGGA	B97-D		121			
	HCTH		122−124			
	M06-L		125			
MHGGA	M05	28	126			
	M05-2X	56	127			
	M06	27	128			
	M06-2X	54	128			
	M06-HF	100	129, 130			
	TPSSH	10	131			
LRC	CAM-B3LYP		132			
	LC-wPBE		133−135			
	wB97XD		136			

In recent years, many theoretical works based on DFT have appeared in the literature dealing with the QDs properties. In particular, most of those focus their attention on the group II−VI type, here denoted as MX, where M stands for a metal belonging to group 12, such as Cd or Zn, and X for a chalcogen atom, like S, Se, and Te. These QDs are very common and are currently employed in many experimental and commercial laboratories. In this article, we will pay attention only to this specific set of compounds. In Table 1, we provide a summary of the computational works carried out so far. Note that a more complete and detailed list is provided in the Supporting Information. The eye-catching feature is how the CdSe QDs are the most studied followed by ZnS. This result however reflects the experimental measurements as these two types of nanocrystals are usually considered as prototypical QDs.

While conceptually simple, DFT depends on several variables that need to be taken into account when tackling a given system. The user of this methodology usually faces two critical choices that can lead to losses or gains in accuracy: (i) the choice of the exchange-correlation functional and (ii) the choice of the basis set expansion. In Table 1, we have collected the articles that have been written so far on group II−VI QDs sorted by DFT functional and basis set. It is interesting to note that the majority of these works have been carried out using the B3LYP functional, with 27 papers, followed by PBE with 14, and 11 for PW91PW91. Regarding basis sets, the most used is

dx.doi.org/10.1021/ct400513s | J. Chem. Theory Comput. 2014, 10, 76−89

the LANL2DZ, which includes effective potentials in the core to reduce the computational effort, included in a total of 16 articles. A close look at these statistics shows that most of these works are based on a widespread standard combination of DFT functional and basis set, rather than on their systematic calibration. It is worthy to mention, however, that a few works have attempted to compare the performance of a small set of DFT functionals.[26,27]

Our purpose is to assess the quality of 26 DFT functionals (Table 2), including also less used meta-generalized gradient approximation and long-range corrected functionals. Because semiconductor nanocrystals are mostly known for their optoelectronic properties, we paid particular attention to building a benchmark data set that incorporates the most relevant excited states of several types of QDs. To establish a more robust database, we have also added in the data set spectroscopic ground state properties like bond lengths and vibrational frequencies. Although real nanocrystals obviously present larger sizes than those employed in this work, we have constructed $(MX)_6$ model systems (Figure 1) that are small enough to be tackled by very accurate *ab initio* methodologies to obtain the best and most accurate estimates of their excited states and geometric parameters. This same benchmark database has been used to evaluate the quality of eight basis sets. The $(MX)_6$ models have been constructed by cutting a wurtzite lattice, whose existence has been proved recently by Schelly.[137]

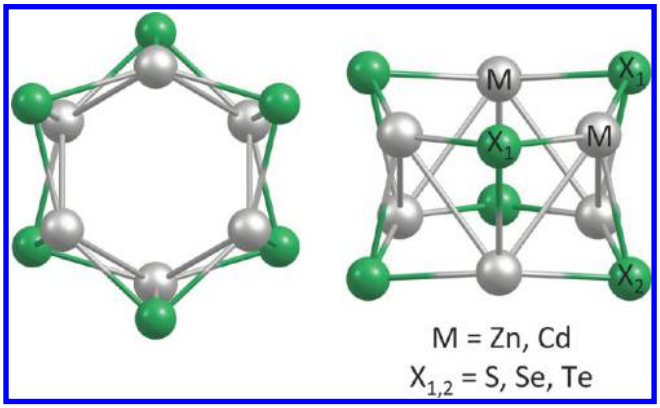

Figure 1. Prototypical $(MX)_6$ structure shown from two different sides.

The present paper is structured as follows. In section 2, we provide detailed insights on how we build the benchmark database and the procedure that is used to assess the accuracy of several DFT functionals and basis sets. In section 3, a description of the results on various nanosize systems is presented. Finally, in section 4, we conclude our work and provide some hints for future theoretical investigations on II–VI QDs.

2. COMPUTATIONAL METHODOLOGY

2.1. Benchmark Set. In a first step, we have attempted to employ very accurate methodologies, like coupled-cluster methodology with single and double excitations perturbatively corrected with triple excitations, CCSD(T),[28] or the complete active space with second-order perturbation method, CASPT2,[29,30] to construct the benchmark database; however we found these approaches impractical for the large computational requirements. We decided thus to switch to approximated coupled cluster methodologies like the resolution-of-identity equation of motion second-order approximate coupled cluster, RI-EOM-CC2, for excited states,[31] while ground state properties have been estimated using second-order perturbation theory, the RI-MP2 method.[32] RI stands for resolution of identity, which is an accelerated algorithm to compute the two-electron coulomb integrals lying in the Hamiltonian.[33] A large def2-TZVPP basis set has been employed to minimize the errors stemming from the finite size of the basis set expansion. Usually, RI-EOM-CC2/def2-TZVPP may suffer from errors in reproducing accurately excited states; therefore we made a preliminary calculation on a selected few low-lying excited states of $(CdSe)_6$ with the CASPT2 method. These results show the satisfactory agreement between CASPT2 and RI-EOM-CC2; therefore we chose the latter throughout the benchmark tackled in this paper.

The main bond distances and bond angles of the optimized $(MX)_6$ model compounds are shown in Table 2, while their vibrational frequencies are presented in Table 3. Finally, in Table 4 we have listed the most characteristic lowest-lying excitation energies of these species.

Table 3. Computed MX (M = Cd, Zn; X = S, Se, Te) Structural Parameters at the RI-MP2/def2-TZVPP Level of Theory[a]

quantum dot, QD	$(ZnS)_6$	$(ZnSe)_6$	$(ZnTe)_6$	$(CdS)_6$	$(CdSe)_6$	$(CdTe)_6$
$M-X_1$	2.265	2.382	2.571	2.426	2.537	2.715
$M-X_2$	2.412	2.516	2.680	2.663	2.757	2.904
M–M	2.776	2.823	2.875	3.121	3.156	3.186
X_1-M-X_1	140.0	140.0	138.7	144.9	145.3	144.5
$M-X_1-M$	94.5	92.3	88.6	102.0	91.1	88.0
X_1-M-X_2	102.6	104.2	107.0	99.0	100.7	103.5

[a]Bond distances are expressed in Å, angles in degrees.

Table 4. Computed MX (M = Cd, Zn; X = S, Se, Te) Vibrational Frequencies at the RI-CC2/def2-TZVPP Level of Theory[a]

quantum dot, QD	$(ZnS)_6$	$(ZnSe)_6$	$(ZnTe)_6$	$(CdS)_6$	$(CdSe)_6$	$(CdTe)_6$
$1e_g$	80	66	48	57	49	39
$1e_u$	86	66	53	58	49	41
$1a_{1g}$	114	95	69	73	66	55
$1a_{2u}$	119	106	90	82	75	59
$2e_g$	127	100	80	86	70	58
$1a_{1u}$	140	102	74	95	75	64
$2e_u$	158	126	104	108	92	75
$2a_{1g}$	167	132	114	119	101	81
$3e_g$	200	151	118	152	113	98
$3e_u$	198	156	140	159	111	96
$3a_{1g}$	225	173	148	190	128	100
$2a_{2u}$	229	146	105	201	133	111
$4e_g$	309	198	164	284	174	131
$4e_u$	316	194	145	289	177	132
$3a_{2u}$	328	236	205	292	192	145
$1a_{2g}$	335	256	214	298	217	180
$4a_{1g}$	336	207	160	310	192	159
$2a_{1u}$	365	273	231	325	230	192
$5e_g$	387	301	258	337	249	212
$5e_u$	391	303	259	342	251	212

[a]Frequencies are given in cm^{-1}.

dx.doi.org/10.1021/ct400513s | J. Chem. Theory Comput. 2014, 10, 76–89

Table 5. Lowest MX (M = Cd, Zn; X = S, Se, Te) Singlet Excited States Computed at the RI-CC2/def2-TZVPP Level of Theory[a]

quantum dot, QD	$(ZnS)_6$	$(ZnSe)_6$	$(ZnTe)_6$	$(CdS)_6$	$(CdSe)_6$	$(CdTe)_6$
$1e_g$	3.45 (0.0000)	3.11 (0.0000)	2.54 (0.0000)	2.89 (0.0000)	2.71 (0.0000)	2.38 (0.0000)
$1a_{2u}$	3.74 (0.0346)	3.41 (0.0200)	2.88 (0.0034)	3.22 (0.0658)	3.02 (0.0468)	2.67 (0.0130)
$1e_u$	4.43 (0.0056)	4.05 (0.0035)	3.38 (0.0002)	3.74 (0.0030)	3.57 (0.0002)	3.19 (0.0004)
$2e_g$	4.36 (0.0000)	4.05 (0.0000)	3.54 (0.0000)	3.83 (0.0000)	3.65 (0.0000)	3.28 (0.0000)
$1a_{2g}$	4.40 (0.0000)	3.93 (0.0000)	3.15 (0.0000)	3.92 (0.0000)	3.63 (0.0000)	3.09 (0.0000)
$2e_u$	4.64 (0.0858)	4.27 (0.0329)	3.58 (0.0287)	3.95 (0.0177)	3.71 (0.0037)	3.22 (0.0221)
$3e_g$	4.83 (0.0000)	4.46 (0.0000)	3.99 (0.0000)	3.97 (0.0000)	3.70 (0.0000)	3.39 (0.0000)
$3e_u$	4.67 (0.0015)	4.34 (0.0311)	3.74 (0.0127)	4.03 (0.1351)	3.84 (0.1145)	3.47 (0.0330)
$1a_{1g}$	4.62 (0.0000)	4.44 (0.0000)	3.80 (0.0000)	4.15 (0.0000)	3.88 (0.0000)	3.37 (0.0000)

[a]Transition energies and oscillator strengths, in parentheses, given in eV and a.u., respectively.

2.1. Assessment of DFT Methodologies against the Benchmark Database. The reference data set defined in the previous section is used to assess computationally cheaper methodologies and to select those that provide results that are in closer agreement with our best estimates. In this work, we are mostly interested in benchmarking DFT exchange-correlation (XC) functionals; however, this reference set may be used in the future to assess other computational approaches.

Apart from the functionals, DFT calculations depend also on the size of the basis set employed and the choice of relativistic approximations, with the latter being important thanks to the presence of heavy atoms like Cd or Te in the reference compounds. Because of this, we decided to follow a two-step approach to perform our benchmark: (i) first we assessed the performance of several basis sets, core potentials, and relativistic approximations on one specific system; (ii) then we chose the best combination provided by point (i) to assess the contribution of different DFT functionals on a much larger selection of systems.

To establish the fairness of our results, we followed optimized benchmark recipes that have been made available by other authors.[34] A few quantities are of relevance to assess the accuracy of each DFT functional (or basis set): (i) The mean unsigned errors (MUE) provide the magnitude of the deviation of a given DFT exchange-correlation functional, XC (or basis set, BS), $MUE[XC(or\ BS)]_{type}$ for a specific "type" parameter, for example; bond distance, $MUE[XC(or\ BS)]_{bond}$; vibrational frequency, $MUE[XC(or\ BS)]_{vib}$; or excited states, $MUE[XC(or\ BS)]_{exc}$, from the reference values, independent of the sign. (ii) The average MUE ($AMUE_{type}$) is the average error spread among all DFT methodologies (or basis sets) for a given parameter. (iii) The normalized mean unsigned errors are defined as $NMUE[XC(or\ BS)]_{type} = MUE[XC(or\ BS)]_{type}/AMUE_{type}$ (type = bond, vib, exc). The NUMEs provide a normalized error value of a given DFT functional (or basis set) for a specific parameter and are independent of the units employed. Finally, (iv) the balanced mean unsigned error, expressed by $BMUE[XC(or\ BS)] = (NMUE[XC(or\ BS)]_{bond} + NMUE[XC(or\ BS)]_{vib} + NMUE[XC(or\ BS)]_{exc})/3$, indicates the overall performance of a DFT functional (or basis set) against all parameters, independently of the units.

2.2. Basis Sets, Core Potentials, and Relativistic Approximations. Several types of basis sets have been benchmarked against one reference system, the $(CdSe)_6$, by performing DFT calculations with a selected number of exchange-correlation functionals: PBE, PBE0, M06-L, and CAM-B3LYP. Both Cd and Se are "heavy" atoms showing important relativistic effects that have been taken into account via scalar approximations. Spin−orbit (SO) coupling contribution is not considered here, as all QDs of this study are closed shell systems. Scalar relativity has been tested using two approaches, the effective-core potentials (ECPs) and the all-electron zeroth-order regular approximation (ZORA). ECPs are integrated into the Gaussian basis sets LANL2DZ, SBKJC, def2-SV(P), and def2-TZVPP, which are the main basis sets considered in this benchmark. All-electron Slater type basis sets, namely DZ and TZ2P, have been employed for the calculations based on the ZORA approximation. In the case of DZ, we have also tested the effect of using frozen core approximation, i.e., freezing the atomic orbital coefficients up to 3d (small-core) and 4p (large-core) for Cd and up to 3p (small-core) and 4p (large-core) for Se. Beware that the def2 basis set library is of all-electron type for Zn, O, and S, while it includes ECPs for Cd, Se, and Te by default. This is not the case for SBKJC and LANL2DZ that always include ECPs.

2.3. Exchange-Correlation DFT Functionals. The performance of several popular exchange-correlation (xc) functionals has been tested on both the $(ZnX)_6$ and $(CdX)_6$ (X = S, Se, Te) clusters. We divided our density functional test set into five main groups (see also Table 2): (i) The first includes "pure" xc functionals constructed from the generalized gradient approximation (GGA); i.e., they are influenced by both the electron density and the gradient of electron density: PBE, BLYP, BPW91, BP86, G96LYP, mPWLYP, and OLYP. (ii) The second group is composed of GGA xc functionals, which also include a given percentage of Hartree−Fock exchange. This set is identified as hybrid GGA (HGGA) and includes the B1LYP, B3LYP, mPW1PW91, O3LYP, B97-2, PBE0, and X3LYP functionals. (iii) The third group is formed by GGA functionals that include a dependence on the kinetic energy densities and are called meta-GGA (MGGA): M06-L, HCTC, and B97D. (iv) The fourth is composed of meta-GGA functionals including a percentage of Hartree−Fock exchange and are identified as meta-HGGAs (MHGGA): M06, M06-HF, M06-2X, M05, M05-2X, and TPSSH. (v) The fifth and last group is determined by those functionals that preserve their identity at short-range but incorporate 100% Hartree−Fock exchange at long-range, in order to correct the distance dependence of charge-transfer excitations. These functionals, also called long-range corrected, or LRC hereafter, have been employed in this benchmark in three flavors: LC-ωPBE, CAM-B3LYP, and ωB97XD.

The basis set chosen for all of these calculations is the def2-SV(P) basis set that incorporates relativistic effects through the Stuttgart relativistic core potentials. As we will see in the text, this basis set represents the best compromise in terms of

dx.doi.org/10.1021/ct400513s | J. Chem. Theory Comput. 2014, 10, 76−89

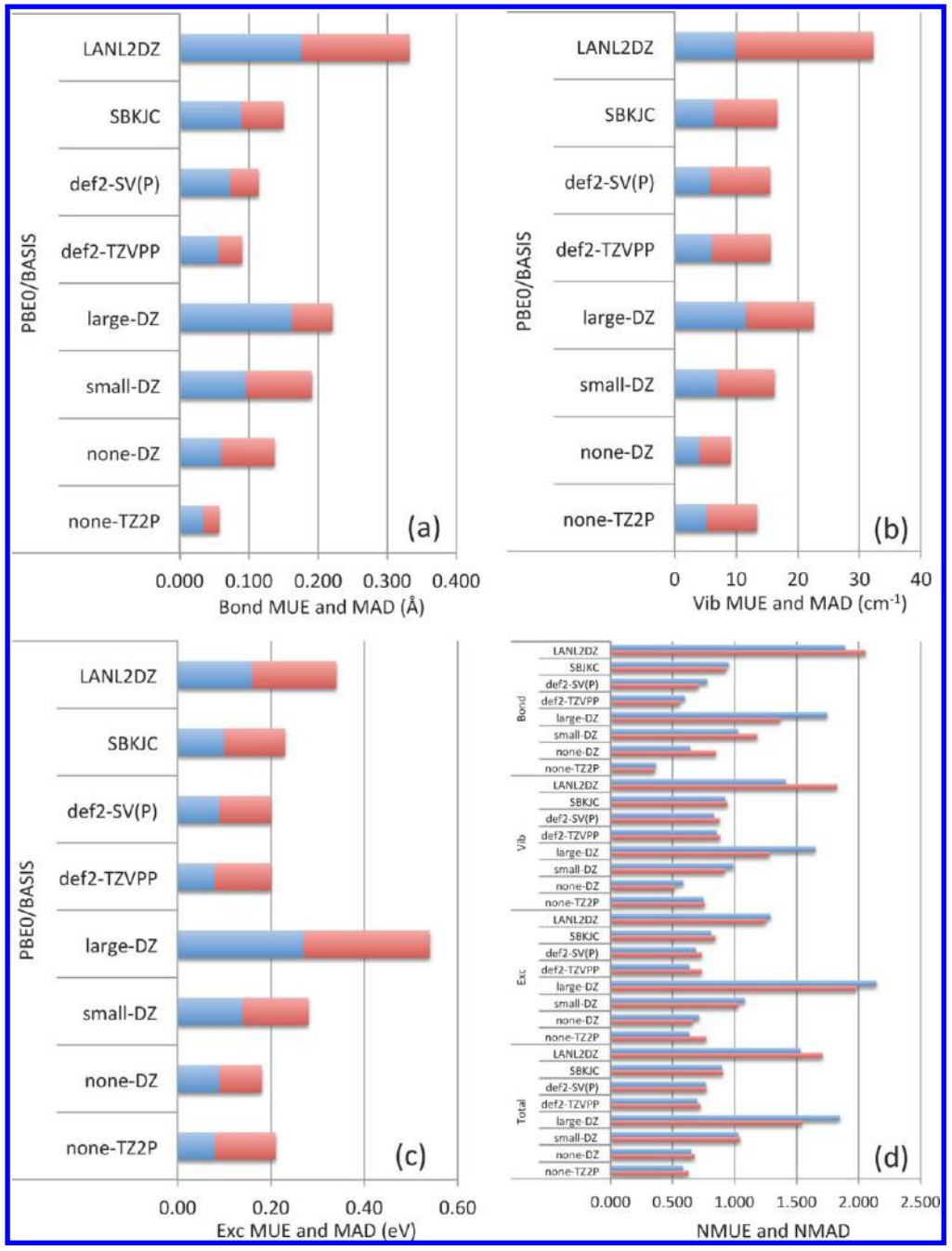

Figure 2. Computed mean-unsigned errors (MUEs; in blue) and maximum deviations (MADs; in red) of several basis sets associated with the MX (M = Cd, Zn; X = S, Se, Te) spectroscopic parameters using the PBE0 exchange-correlation functional. (a) bond distances (Å), (b) vibrational frequencies (cm^{-1}), (c) excitation energies (eV). (d) Normalized mean unsigned errors (NMUEs; in blue) and normalized maximum absolute deviations (NMADs; in red) for each parameter (bonds, vibrations, excitations). The balanced mean unsigned errors (BMUEs; in blue) and balanced maximum errors (BMADs; in red) are also computed at the bottom of panel (d) by averaging the errors over all parameters. Note that the normalization step for the computation of BMUEs allows NMUEs to be, in some cases, larger than NMADs.

computational requirements and accuracy for tackling larger systems.

2.4. Details on the Program Packages Used. Calculations have been carried out using several computational packages. The reference data set has been collected using Turbomole 6.4[35] as it provides the RI-EOM-CC2 and the RI-MP2 methodologies. All DFT calculations using Gaussian basis sets have been performed with Gaussian 09,[36] while ADF2012.01[37] has been used to calculate the effect of the DZ and TZ2P basis within the ZORA approximation. All references for the DFT functionals, basis sets, and ECPs are provided in Table 2.

3. RESULTS AND DISCUSSIONS

3.1. Benchmark of Basis Sets, Core Potentials, and Relativistic Approximations. As anticipated earlier, the first step is to benchmark a selected number of basis sets, incorporating relativistic approximations with ECP or all-electron ZORA. The quality of a given basis set for a given parameter (bond distances, vibrational frequencies, and excited

dx.doi.org/10.1021/ct400513s | J. Chem. Theory Comput. 2014, 10, 76−89

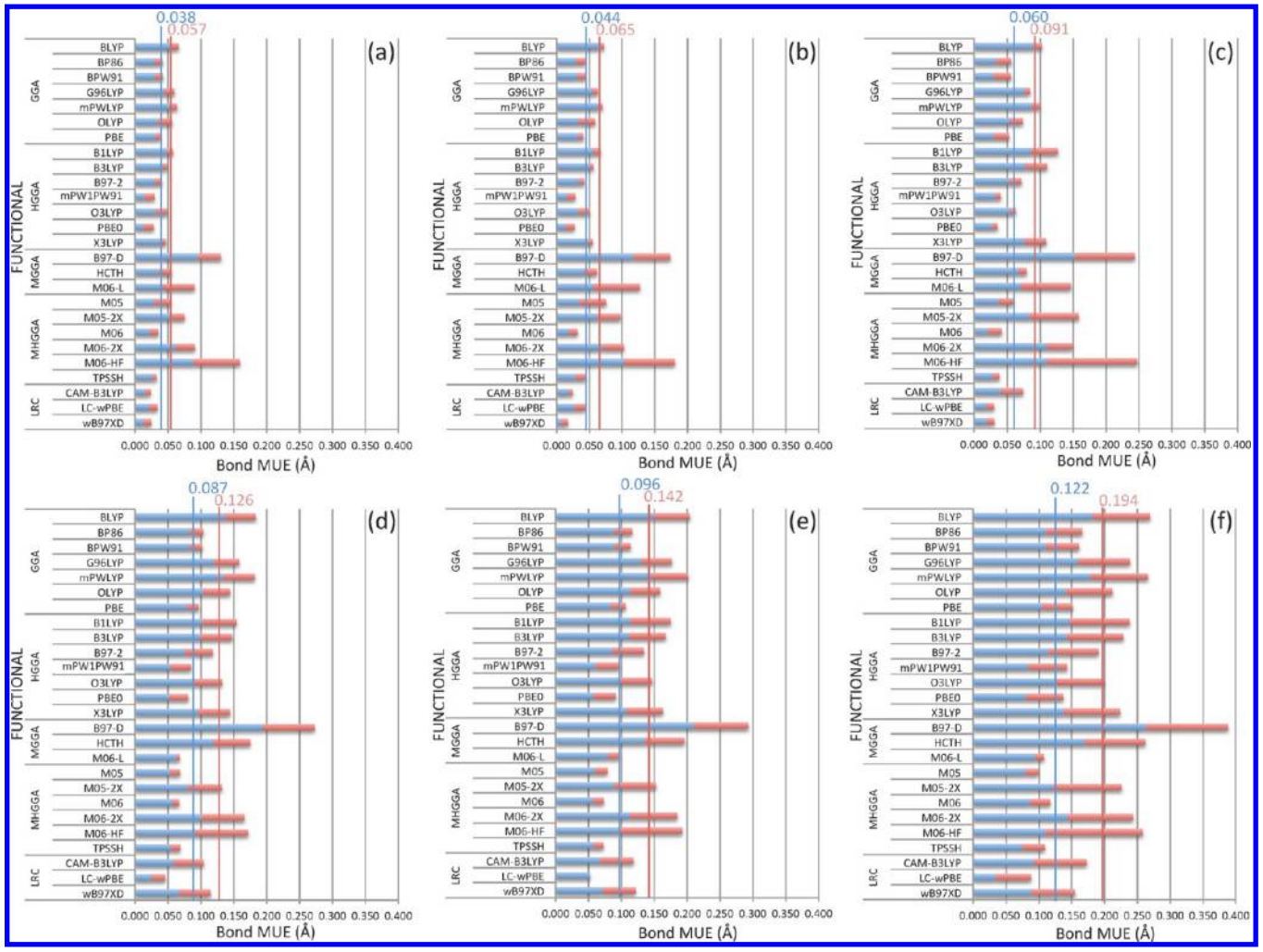

Figure 3. Computed mean-unsigned errors (MUEs; in blue) and maximum deviations (MADs; in red) of several exchange-correlation (xc) DFT functionals, in conjunction with the MX (M = Cd, Zn; X = S, Se, Te) bond lengths (in Å). (a) $(ZnS)_6$, (b) $(ZnSe)_6$, (c) $(ZnTe)_6$, (d) $(CdS)_6$, (e) $(CdSe)_6$, and (f) $(CdTe)_6$. The vertical lines indicate average mean unsigned error (AMUE; in blue) and the average maximum absolute deviation (AMD; in red).

states) is evaluated with the MUEs. To obtain a more complete statistical set of data, we computed the same properties using different functionals, PBE, PBE0, M06-L, M06-2X, and CAM-B3LYP, each representing a different description of the exchange-correlation term. In Tables 3−5, we have listed the results of our benchmark by displaying the reference data set computed at the RI-MP2 (for geometry and vibrational frequencies) and EOM-CC2 (for excited states) levels of theory. Figure 2 summarizes the performance of the DFT/PBE0 approach. In the Supporting Information, we also include the results from the other functionals. Regarding the bond parameters, the TZ2P in combination with the PBE0 provides the best performance, with a MUE of 0.034 Å and a maximum deviation of 0.057 Å. The next more accurate values are achieved by the def2-TZVPP in combination with M06-L, M06-2X, and CAM-B3LYP, and also by PBE/TZ2P. In general, as expected, the largest basis sets provide the most accurate values. This trend is however changed for the normal modes values where the PBE0/DZ and PBE0/def2-SV(P) are estimated to be closer to the reference values. Regarding the excited states benchmark, it is interesting to note that the best performing basis set varies a lot with the type of DFT functional. In particular, the computationally cheap SBKJC basis set provides surprising results by outperforming, in some cases, larger basis sets. For example, the combination of SBKJC with M06-2X gives a MUE of 0.10 eV, better than 0.17 eV of def2-TZVPP and 0.22 eV of all-electron ZORA TZ2P.

A better view of the overall performance of each basis set is the balanced mean-unsigned error (BMUE), i.e., a unitless term that takes into account the global average effect of bond distances, vibrations, excited states, and different DFT functionals. The results are presented in Figure 2d. It is clear that the best performing basis set is the def2-TZVPP, with a BMUE of 0.808 and a balanced maximum error of 0.781. The worst performance is given by the all-electron DZ basis set, in which a large frozen core has been chosen, with a BMUE of 1.333. Most notably, the LANL2DZ basis, which has been widely used in previous works on QDs, performs very unsatisfactorily, being the second worst basis in the benchmark with a BMUE of 1.247. Breaking down the BMUE in terms of its components, the LANL2DZ has its worst behavior with the geometric parameters, while for excited states it performs only slightly better. Usually, the LANL2DZ is employed for its computational efficiency versus a much larger basis set, like def2-TZVPP; however we must warn of the quality of its results. A very good alternative is the SBKJC basis, which has a BMUE of

dx.doi.org/10.1021/ct400513s | J. Chem. Theory Comput. 2014, 10, 76−89

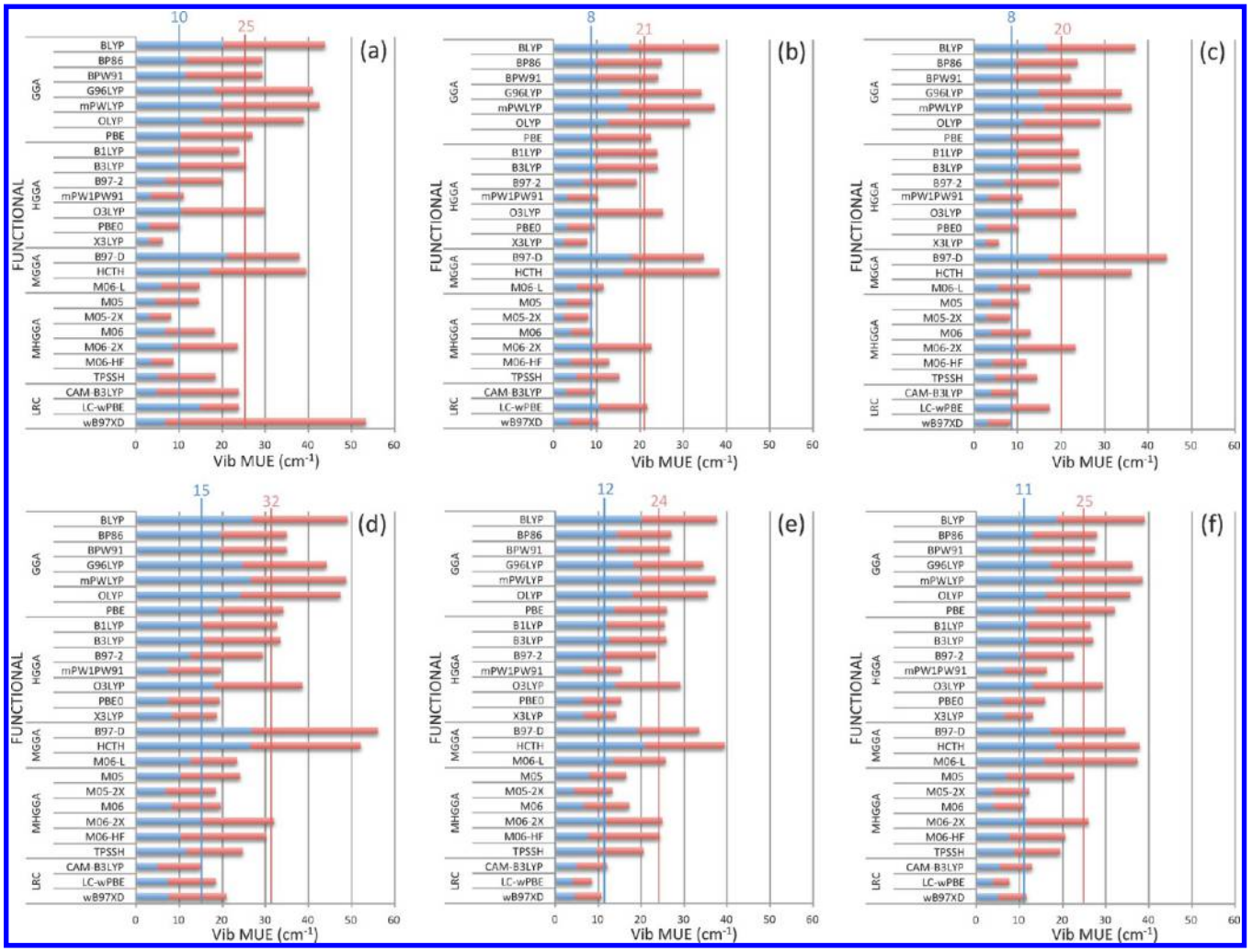

Figure 4. Computed mean-unsigned errors (MUEs; in blue) and maximum deviations (MADs; in red) of several exchange-correlation (xc) DFT functionals, in conjunction with the MX (M = Cd, Zn; X = S, Se, Te) normal modes (in cm^{-1}). (a) $(ZnS)_6$, (b) $(ZnSe)_6$, (c) $(ZnTe)_6$, (d) $(CdS)_6$, (e) $(CdSe)_6$, and (f) $(CdTe)_6$. The vertical lines indicate average mean unsigned error (AMUE; in blue) and the average maximum absolute deviation (AMD; in red).

0.909, only slightly higher than the def2-TZVPP. Moreover, this same basis set, as anticipated earlier, has by far the best performance for excited states, with a $NMUE[SBKJC]_{exc}$ as low as 0.805, much lower than the second best given by def2-TZVPP with 0.922. Another very promising basis set for its accuracy and computational efficiency is def2-SV(P), which has a BMUE of only 0.861 and has the second overall best behavior.

Among the all-electron Slater basis set, and within the relativistic ZORA approximation, TZ2P provides the lowest, and therefore most accurate, BMUE value (0.892), followed by the all-electron DZ (0.943). Notably, freezing the core orbitals leads to an important deterioration of the results, especially for the large core DZ, which is suggested to be avoided in all cases.

3.2. Assessment of Exchange-Correlation DFT Functionals. In Figures 3−5 (and Tables S5, S7, and S9) we have listed the computed MUEs of several DFT exchange-correlation functionals at the def2-SV(P) level of theory for geometrical parameters, vibrational frequencies, and excited states of Cd and Zn chalcogenide clusters. In the Supporting Information, we have also tabulated the NMUEs (Tables S6, S8, and S10). In Figure 6, we have collected the $BMUE[XC]_{type}$ for type = bond, vib, and exc, collected by averaging the results over all nanoclusters employed, i.e., $BMUE[XC]_{type} = (NMUE-[XC]_{type\text{-}CdS} + NMUE[XC]_{type\text{-}CdSe} + ... + NMUE[XC]_{type\text{-}ZnTe})/6$. This provides an outlook of the general performance of each DFT functional for all molecular species. In Figure 6d, we also show the overall BMUE averaged against all parameters and all QDs.

Regarding geometrical parameters, the best functional is TPSSH, followed by M06, LC-ωPBE, M05, and PBE0 (Figure 6a). All these functionals include a certain degree of HF exchange and usually are computationally expensive for structural optimizations, especially when used for larger systems. A possible valid alternative is the "pure" local PBE functional, which shows a $BMUE_{bond}$ of just 0.608, meaning that it performs better than the majority of the functionals, including some of the hybrid ones. A similar trend can be found in the vibrational parameters, where the best functional is PBE0, which includes 25% of HF exchange and has a $BMUE_{vib}$ of 0.437, followed by M05 and TPSSH. Again, hybrid functionals provide the most accurate values against the reference benchmark. In this case, almost all local GGAs perform worse than the average, with the only exception of PBE, which has $BMUE_{vib}$ of 1.002, even though it is quite close

dx.doi.org/10.1021/ct400513s | J. Chem. Theory Comput. 2014, 10, 76−89

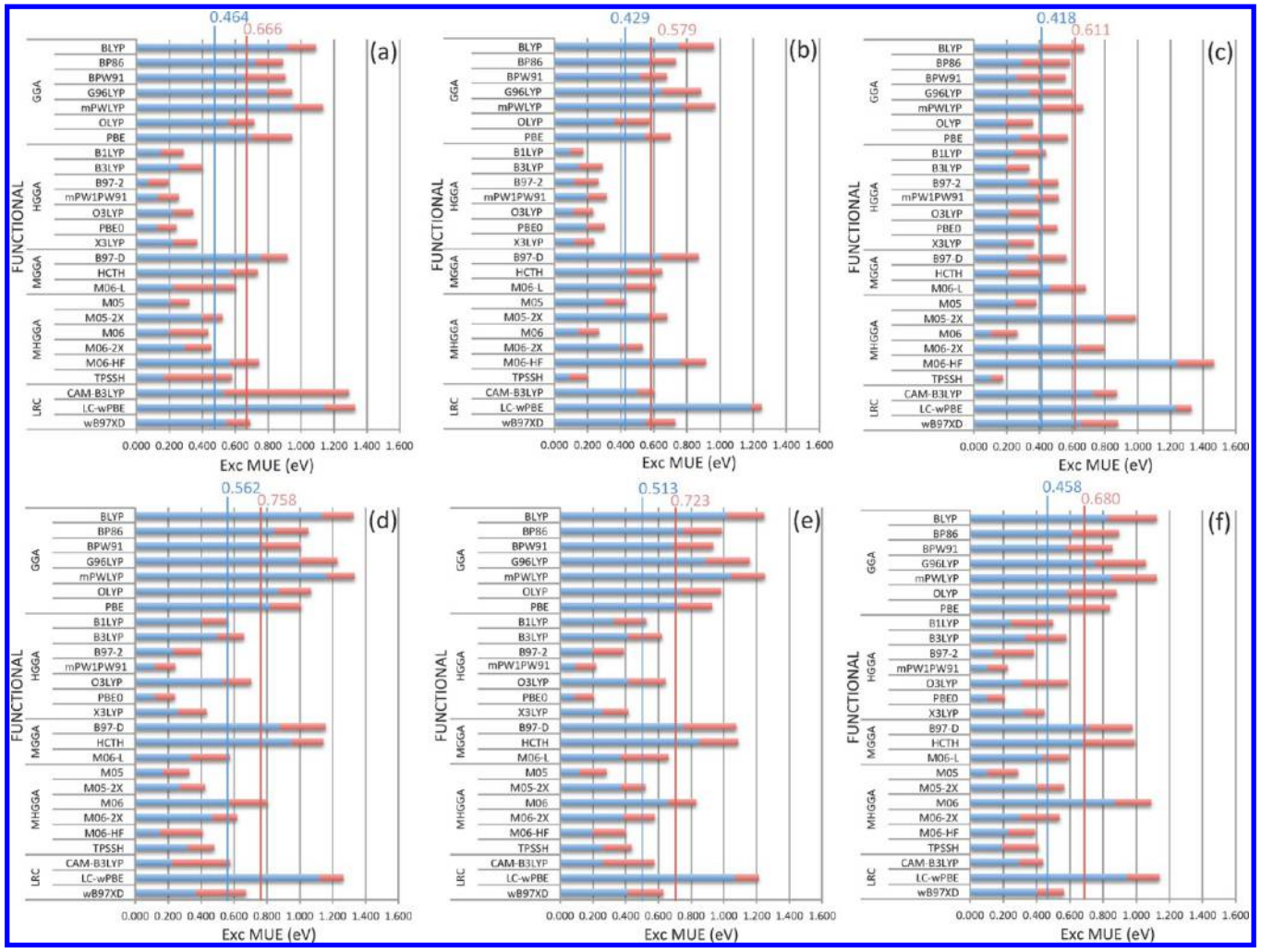

Figure 5. Computed mean-unsigned errors (MUEs; in blue) and maximum deviation (MADs; in red) of several exchange-correlation (xc) DFT functionals, in conjunction with the MX (M = Cd, Zn; X = S, Se, Te) excitation energies (in eV). (a) $(ZnS)_6$, (b) $(ZnSe)_6$, (c) $(ZnTe)_6$, (d) $(CdS)_6$, (e) $(CdSe)_6$, and (f) $(CdTe)_6$. The vertical lines indicate average mean unsigned error (AMUE; in blue) and the average maximum absolute deviation (AMD; in red).

to the median 1.000. Among MGGA functionals, the M06-L represents a sound replacement, with a $BMUE_{vib}$ of 0.785.

More interestingly, the PBE0 functional also provides the most accurate description of the lowest nine excited states with an overall $BMUE_{exc}$ of 0.370. Other highly performing functionals are mPW1PW91, B97-2, TPSSH, and M05. These methods all belong to the hybrid group, with HF exchange contribution varying from 10% to 28%. Pure GGA functionals have very poor performance, and even the best one, BPW91, produces a $BMUE_{exc}$ of 1.204. In terms of absolute energies, for example for the $(CdS)_6$ cluster, this corresponds to a systematic MUE of 0.78 eV, which is not at all satisfactory. This result is somewhat worrying as pure GGAs are more efficient computationally. Also in this case, the M06-L, which has no HF exchange, describes the reference values with a $BMUE_{exc}$ of 0.803. Despite not being the best overall, it might represent a good compromise in terms of accuracy and efficiency for studying large clusters. The origin of the bad performance of local GGA functionals can be ascribed to the type of excited states involved in these clusters. These excitations are usually exciton-like, with the formation of the so-called hole−electron pair and the consequent shift of charge that traduces into a long-range $1/r$ Coulombic attraction between the hole and the electron. The failure of pure TDDFT lies in the lack of the exact HF exchange term that in linear response theory is directly connected to the correct $1/r$ asymptotic behavior. Moreover, these charge transfer states are also severely underestimated as a consequence of self-interaction error. In our work, we systematically demonstrate the higher performance of hybrid functionals, which include a given percentage of HF exchange.

Overall, the functional that predicts more accurately all the parameters over all compounds considered here is PBE0, with a $BMUE_{total}$ of 0.437. This is followed closely by mPW1PW91, M05, and TPSSH. As expected, the hybrid functionals HGGA and MHGGA outperform pure GGAs and MGGAs, with the latter being better than pure GGAs.

The results presented so far take into consideration the prediction of xc-functionals over the whole set of compounds. It is however of particular interest to look at their behavior for specific systems. To keep the description simple, in the analysis, we will focus only on the prediction of the excitation energies, as presented in Figure 5. The discussion can be easily extended to the other computed properties. For the whole set of cadmium chalcogenides $(CdS)_6$, $(CdSe)_6$, and $(CdTe)_6$, the PBE0 is the overall best functional by providing excited state

dx.doi.org/10.1021/ct400513s | J. Chem. Theory Comput. 2014, 10, 76−89

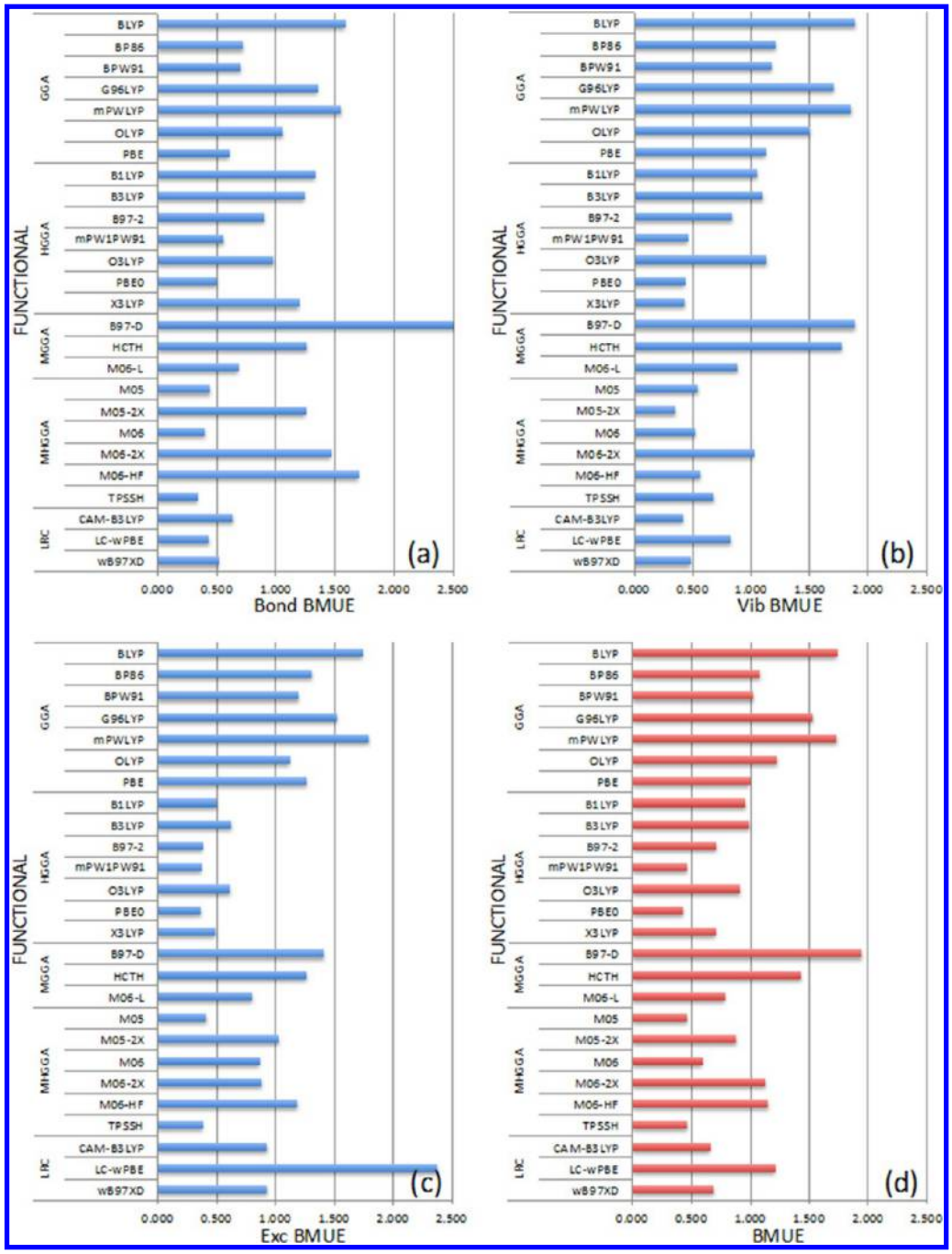

Figure 6. BMUEs for (a) bond lengths, (b) vibrational frequencies, and (c) excitation energies averaged over all nanoclusters studied. (d) Total BMUEs averaged over panels (a), (b), and (c).

energies very close to the reference RI-EOMCC2 values and MUEs of 0.120 eV (CdS), 0.090 eV (CdSe), and 0.099 eV (CdTe), respectively. The next best functional is the mPW1PW91, followed by other MHGGA's, like M06-HF and M05. A look at the correlation diagrams in Figure 7 indicates that PBE0 predicts an oscillating behavior above and below the reference excitation energies, providing, in any case, an excellent agreement with the benchmark reference. A similar behavior is found for the other best functionals indicated here and for the other CdX compunds. Pure GGAs, however, always underestimate the excitation energies with deviation from the reference values of up to 0.9−1.0 eV for all CdX systems. Among the MGGA functionals, the M06-L behaves much better than pure GGAs. On the other hand, LRC functionals overcorrect the exciton interaction by providing excitation energies systematically larger than the reference of about 0.3 eV (CAM-B3LYP) or up to 0.9 eV (LC-wPBE).

One of the key findings in moving to the ZnX chalcogenides is that the situation is somewhat changed. The PBE0 still performs well, but less than in the CdX compounds. In particular, for ZnTe, it gives a MUE as high as 0.374 eV, which is still below the median but much lower performing than for CdX (or even ZnS and ZnSe). In all ZnX species, the PBE0 tends to overestimate all the excitation energies (see Figure 7) of about 0.3−0.4 eV. This functional has a 25% HF exchange, the same as mPW1PW91, which suffers from the same

dx.doi.org/10.1021/ct400513s | J. Chem. Theory Comput. 2014, 10, 76−89

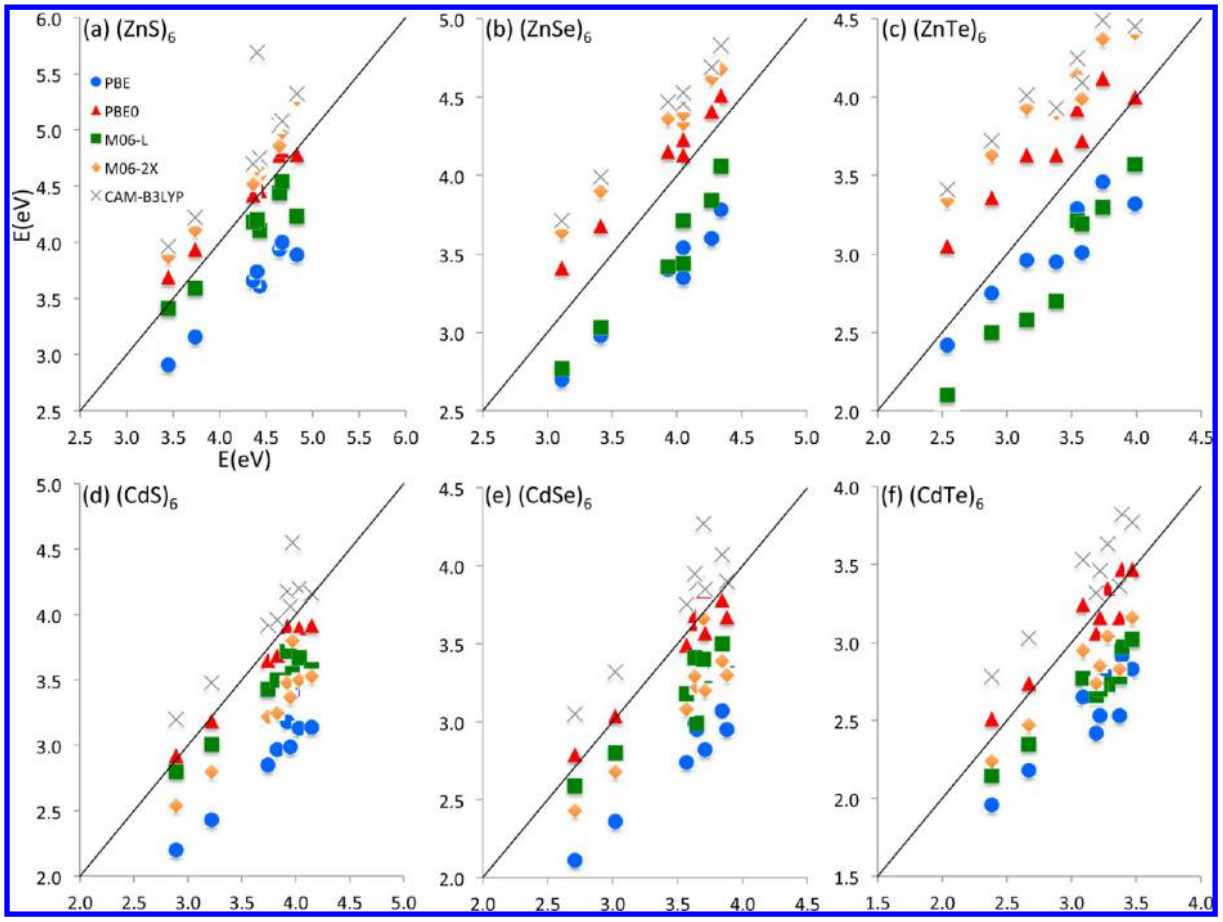

Figure 7. Correlation diagrams for the excitation energies computed with a restricted selection of DFT functionals (y axis) against the reference benchmark (x axis). (a) $(ZnS)_6$, (b) $(ZnSe)_6$, (c) $(ZnTe)_6$, (d) $(CdS)_6$, (e) $(CdSe)_6$, and (f) $(CdTe)_6$.

problems. Notably, reduction of HF exchange leads to better results. Indeed, the TPSSH functional, with only 10% HF exchange, is the best functional for the ZnX series with MUEs of 0.168 eV (ZnS), 0.091 eV (ZnSe), and 0.105 eV (ZnTe). The smaller importance of the exchange term has also the consequence of improving the results of GGA functionals, especially for the ZnTe cluster, where in some cases they perform better than hybrid functionals.

In the excited state benchmark seen so far, we decided to include in the test set also those electronic excitations that are transparent to light (i.e., with zero oscillator strength) in order to have a statistically more meaningful set of reference data. However, in reality, we are interested only in optically active excited states. An important aspect to assess the performance of a DFT functional is therefore to check how it reproduces the convoluted optical spectrum of the reference data, which is shown in shaded gray in Figure 8. In this figure, on the left, we have plotted the convoluted spectra for all DFT functionals for one system, the $(CdSe)_6$ nanocluster. As expected, the best agreement is provided by the hybrid functionals. However, the facets of the reference curve, i.e., a weaker band at lower energies and a more intense one at higher energies, are well reproduced, though with some differences, in all cases. For this reason, we decided to make a rigid shift of all excitation energies for a given DFT functional equivalent to its MUE. In Figure 8, on the right, we have collected the new curves after the shift. Notably, the reference curve is very well aligned with most of the DFT functionals. In particular, the poor performing pure DFT functionals are now able to satisfactorily describe the reference optical spectrum at a fraction of the computational cost, also in comparison with the hybrid functionals.

Another problem that can occur in establishing the quality of a DFT functional in describing the excited states is the starting geometry. It is indeed probable that some of the DFT methodologies employed can produce optimized structures that are far from the reference values and, consequently, lead to poor excitation energies. To assess this, we decided to compute the excited states with all DFT functionals at the reference RI-MP2 geometry. In Figure 9, we show the trend of the MUE along the series of XC functionals. As expected, at the reference geometry, the overall AMUE, i.e., the average mean unsigned error, is lower than the one computed by optimizing each structure with a given functional. In addition, the trend of the MUE at the RI-MP2 geometry follows roughly that of the DFT geometries, with some notable exceptions. Indeed, the B97-2 and especially the B1LYP reduce drastically their MUE and perform as well as the PBE0 functional.

In the Supporting Information, we also depict the convoluted spectra at the RI-MP2 geometry.

4. CONCLUSIONS AND SUGGESTIONS

In this work, we have built a reference database of *ab initio* RICC2/def2-TZVPP ground state parameters like geometries and vibrational frequencies and several excited states for a group of $(MX)_6$ compounds (M = Cd, Zn; X = S, Se, Te). We have tested the accuracy of 26 exchange-correlation functionals

dx.doi.org/10.1021/ct400513s | J. Chem. Theory Comput. 2014, 10, 76−89

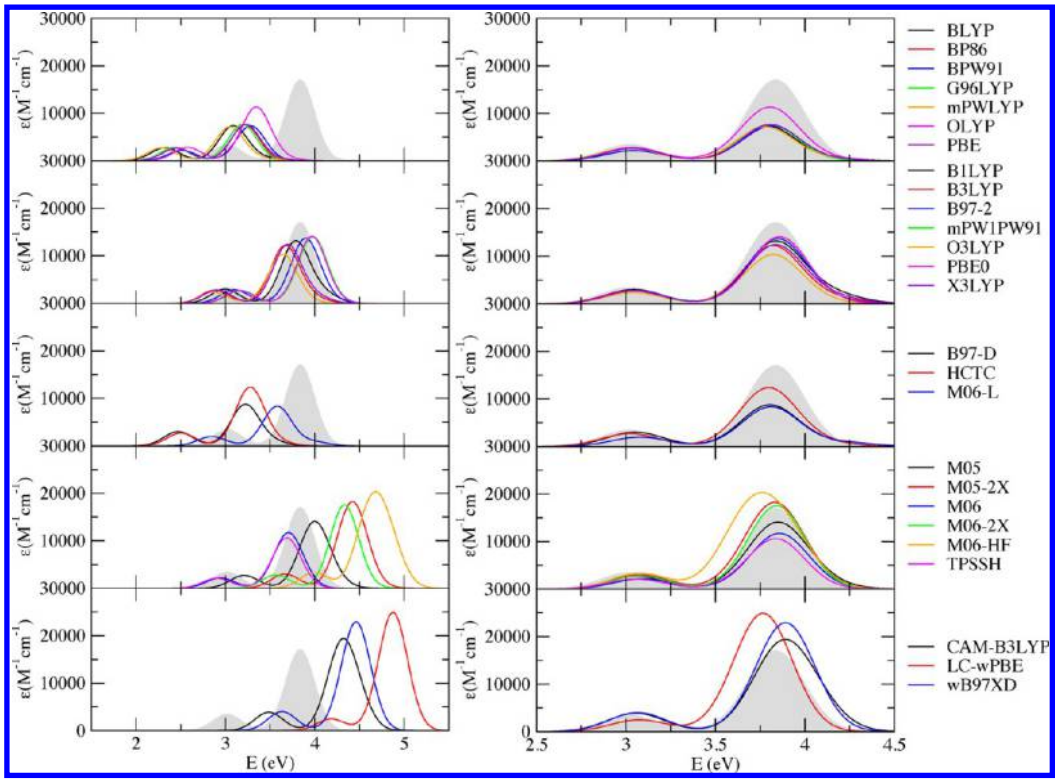

Figure 8. (Left) Simulated absorption spectra of the $(CdSe)_6$ cluster, drawn by a Gaussian convolution with fwhm = 3000 cm^{-1}, calculated taking into account the lowest 20 electronic transitions. Results obtained with the def2-SV(P) functional, on top of the geometries optimized with each functional. The reference EOM-RICC2 spectrum is shown in shaded gray. (Right) DFT spectra are shifted rigidly by their MUE value.

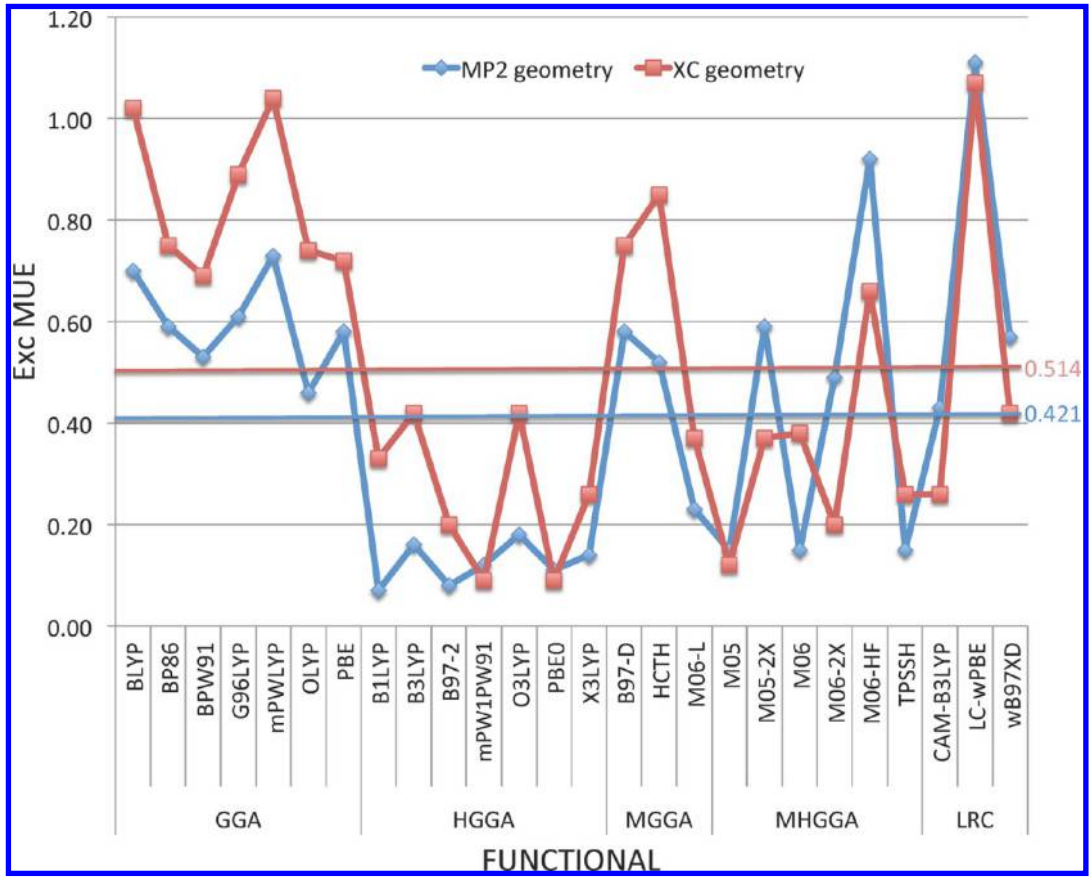

Figure 9. MUEs for the excitation energies computed on the $(CdSe)_6$ complex at the RI-MP2 and DFT geometries.

dx.doi.org/10.1021/ct400513s | J. Chem. Theory Comput. 2014, 10, 76−89

and found out that the hybrid PBE0 is the best performing one, showing a BMUE of 0.437. Other well-behaved functionals usually include HF exchange and, in some cases, also the kinetic energy density. In this group, the M05 and TPSSH have BMUEs of 0.471 and 0.472 very close to PBE0. Local GGA functionals are usually good for structures and normal modes, but for excited states they behave rather poorly. Overall, the best GGA is the PBE with a BMUE of 1.002, while within the MGGAs, the M06-L provides a better value of 0.793.

Regarding the $(CdSe)_6$ cluster, we have also tested the efficiency of several basis sets that incorporate relativistic effects by means of ECPs or ZORA approximations. Overall, the def2-TZVPP with ECPs is the best basis set with a BMUE of 0.808, evaluated for the same set of ground and excited state parameters and a set of five exchange-correlation functionals. The def2-TZVPP, however, requires great computational effort even for small systems, therefore better options are the SBKJC and the def2-SV(P), which have BMUEs of 0.909 and 0.861, respectively. In particular, the SBKJC, which is built with fewer basis functions than the def2-SV(P), performs surprisingly well for excited state calculations by outperforming even the def2-TZVPP basis set.

Finally, we can conclude this article by providing some suggestions for future theoretical work on group II−VI nanoclusters. Realistic QDs are usually large molecules of more than 2 nm in diameter that could easily correspond to structures with more than 200−300 atoms (depending on the type of M and X atoms) and more than 2000−3000 basis functions. These structures have to be first optimized to reach a minimum in the potential energy surface and then used to compute spectroscopic properties, most likely for an infrared or an absorption/emission spectrum. TDDFT calculations would usually require a large amount of memory especially because QDs have a dense manifold of molecular orbitals lying in the HOMO region that could participate in the composition of low-lying excited states. In other words, the larger is the QD, the higher is the number of excitations needed to reproduce the experimental spectrum, and the larger will be the computational effort needed. As a consequence, an approach that will use hybrid functionals, for example PBE0, for geometry optimization and excited state calculations will most likely be prohibitive upon increasing the size of the dot. Within this framework, we foresee two possible workarounds: (1) We have shown that GGA functionals provide reasonable geometries, therefore structural optimizations can be carried out using cheaper methods like PBE. Then, on the optimized structures, a single-point TDDFT calculation using a well-performing hybrid functional could be made (PBE0 standing above all others). In this way, such a sound combination of DFT functionals could provide very reliable results with a reduced computational cost. In preliminary calculations, we have seen that excited states are well reproduced even when the starting structure comes from a different functional than the one used to optimize the structure. (2) Another alternative is to use for the DFT ground state calculations a local GGA density functional as in the previous step and using the same local functional to compute the excited states with TDDFT. Then a rigid shift can be performed on the excitation energies of an amount equivalent to the computed MUE for the given functional. This approach, which is less rigorous than the others, could provide, however, reasonable accuracy with a much reduced computational cost.

■ ASSOCIATED CONTENT

Supporting Information

The full benchmark including MUEs, NMUEs, and BMUEs is provided in explicit form in Tables S1−S12. Simulated absorption spectra of the $(CdSe)_6$ cluster, calculated at the RI-MP2 geometry, and DFT spectra shifted rigidly by their MUE value are shown in Figure S1. This material is available free of charge via the Internet at http://pubs.acs.org.

■ AUTHOR INFORMATION

Corresponding Author

*E-mail: iinfant76@gmail.com.

Notes

The authors declare no competing financial interest.

■ ACKNOWLEDGMENTS

Financial support comes from Eusko Jaurlaritza (IT588-13 and S-PC12UN003) and the Spanish Office for Scientific Research (CTQ2012-38496-C05-01). UPV/EHU is gratefully acknowledged for their generous allocation of computational resources. Support from Ikerbasque is also gratefully acknowledged. J.M.A. would like to thank the Spanish Ministry of Education for funding through a FPU fellowship (AP2009-1514).

■ REFERENCES

(1) Murphy, C. J.; Coffer, J. L. *Appl. Spectrosc.* **2002**, *56*, 16.
(2) Lohse, S. E.; Murphy, C. J. *J. Am. Chem. Soc.* **2012**, *134*, 15607.
(3) Hetsch, F.; Xu, X.; Wang, H.; Kershaw, S. V.; Rogach, A. L. *J. Phys. Chem. Lett.* **2011**, *2*, 1879.
(4) Kamat, P. V. *J. Phys. Chem. C* **2008**, *112*, 18737.
(5) Sargent, E. H. *Nat. Photonics* **2012**, *6*, 133.
(6) Kamat, P. V. *J. Phys. Chem. C* **2007**, *111*, 2834.
(7) Kamat, P. V. *Acc. Chem. Res.* **2012**, *45*, 1906.
(8) Harris, C.; Kamat, P. V. *ACS Nano* **2009**, *3*, 682.
(9) Harris, C.; Kamat, P. V. *ACS Nano* **2010**, *4*, 7321.
(10) Ruberu, T. P. a.; Nelson, N. C.; Slowing, I. I.; Vela, J. *J. Phys. Chem. Lett.* **2012**, *3*, 2798.
(11) Wang, C.; Thompson, R. L.; Baltrus, J.; Matranga, C. *J. Phys. Chem. Lett.* **2010**, *1*, 48.
(12) Abbasi, A. Z.; Amin, F.; Niebling, T.; Friede, S.; Ochs, M.; Carregal-Romero, S.; Montenegro, J.-M.; Rivera Gil, P.; Heimbrodt, W.; Parak, W. J. *ACS Nano* **2011**, *5*, 21.
(13) Aberasturi, D. J. D.; Montenegro, J.-M.; Larramendi, I. R. D.; Rojo, T.; Klar, T. A.; Alvarez-Puebla, R.; Liz-Marza, L. M.; Parak, W. J. *Chem. Mater.* **2012**, *24*, 738.
(14) Nann, T.; Skinner, W. M. *ACS Nano* **2011**, *5*, 5291.
(15) Hildebrandt, N. *ACS Nano* **2011**, *5*, 5286.
(16) Medintz, I. L.; Uyeda, H. T.; Goldman, E. R.; Mattoussi, H. *Nat. Mater.* **2005**, *4*, 435.
(17) Prezhdo, O. V. *Acc. Chem. Res.* **2009**, *42*, 2005.
(18) Smith, A. M.; Nie, S. *Acc. Chem. Res.* **2010**, *43*, 190.
(19) Alivisatos, A. P. *J. Phys. Chem.* **1996**, *100*, 13226.
(20) Alivisatos, A. P. *Science* **1996**, *271*, 933.
(21) Kambhampati, P. *Acc. Chem. Res.* **2011**, *44*, 1.
(22) Voznyy, O.; Thon, S. M.; Ip, A. H.; Sargent, E. H. *J. Phys. Chem. Lett.* **2013**, *4*, 987.
(23) Malet, F.; Gori-Giorgi, P. *Phys. Rev. Lett.* **2012**, *109*, 246402 1.
(24) Yannouleas, C.; Landman, U. *Rep. Prog. Phys.* **2007**, *70*, 2067.
(25) Malet, F.; Mirtschink, A.; Cremon, J. C.; Reimann, S. M.; Gori-Giorgi, P. *Phys. Rev. B* **2013**, *87*, 115146 1.
(26) Yang, P.; Tretiak, S.; Masunov, A. E.; Ivanov, S. *J. Chem. Phys.* **2008**, *129*, 74709.
(27) Albert, V. V.; Ivanov, S. A.; Tretiak, S.; Kilina, S. V. *J. Phys. Chem. C* **2011**, *115*, 15793.
(28) Pople, J. A.; Head-Gordon, M.; Raghavachari, K. *J. Chem. Phys.* **1987**, *87*, 5968.

(29) Andersson, K.; Malmqvist, P. A.; Roos, B. O.; Sadlej, A. J.; Wolinski, K. *J. Phys. Chem.* **1990**, *94*, 5483.
(30) Andersson, K.; Malmqvist, P.-A.; Roos, B. O. *J. Chem. Phys.* **1992**, *96*, 1218.
(31) Hattig, C.; Weigend, F. *J. Chem. Phys.* **2000**, *113*, 5154.
(32) Bernholdt, D. E.; Harrison, R. J. *J. Chem. Phys.* **1998**, *109*, 1593.
(33) Eichkorn, K.; Treutler, O.; Öhm, H.; Häser, M.; Ahlrichs, R. *Chem. Phys. Lett.* **1995**, *240*, 283.
(34) Amin, E. A.; Truhlar, D. G. *J. Chem. Theory Comput.* **2007**, *4*, 75.
(35) Ahlrichs, R.; Bär, M.; Häser, M.; Horn, H.; Kölmel, C. *Chem. Phys. Lett.* **1989**, *162*, 165.
(36) Frisch, M. J.; Trucks, G. W.; Schlegel, H. B.; Scuseria, G. E.; Robb, M. A.; Cheeseman, J. R.; Scalmani, G.; Barone, V.; Mennucci, B.; Petersson, G. A.; Nakatsuji, H.; Caricato, M.; Li, X.; Hratchian, H. P.; Izmaylov, A. F.; Bloino, J.; Zheng, G.; Sonnenberg, J. L.; Hada, M.; Ehara, M.; Toyota, K.; Fukuda, R.; Hasegawa, J.; Ishida, M.; Nakajima, T.; Honda, Y.; Kitao, O.; Nakai, H.; Vreven, T.; Montgomery, J. A.; Peralta, J. E.; Ogliaro, F.; Bearpark, M.; Heyd, J. J.; Brothers, E.; Kudin, K. N.; Staroverov, V. N.; Kobayashi, R.; Normand, J.; Raghavachari, K.; Rendell, A.; Burant, J. C.; Iyengar, S. S.; Tomasi, J.; Cossi, M.; Rega, N.; Millam, J. M.; Klene, M.; Knox, J. E.; Cross, J. B.; Bakken, V.; Adamo, C.; Jaramillo, J.; Gomperts, R.; Stratmann, R. E.; Yazyev, O.; Austin, A. J.; Cammi, R.; Pomelli, C.; Ochterski, J. W.; Martin, R. L.; Morokuma, K.; Zakrzewski, V. G.; Voth, G. A.; Salvador, P.; Dannenberg, J. J.; Dapprich, S.; Daniels, A. D.; Farkas; Foresman, J. B.; Ortiz, J. V.; Cioslowski, J.; Fox, D. J. *Gaussian 09*; Gaussian, Inc.: Wallingford, CT, 2009.
(37) te Velde, G.; Bickelhaupt, F. M.; Baerends, E. J.; Fonseca Guerra, C.; van Gisbergen, S. J. A.; Snijders, J. G.; Ziegler, T. *J. Comput. Chem.* **2001**, *22*, 931.
(38) Schrier, J.; Demchenko, D. O.; Wang, L. W.; Alivisatos, A. P. *Nano Lett.* **2007**, *7*, 2377.
(39) Nanavati, S. P.; Sundararajan, V.; Mahamuni, S.; Kumar, V.; Ghaisas, S. V. *Phys. Rev. B* **2009**, *80*, 1.
(40) Joswig, J.-O.; Springborg, M.; Seifert, G. *J. Phys. Chem. B* **2000**, *104*, 2617.
(41) Sarkar, P.; Springborg, M. *Phys. Rev. B* **2003**, *68*, 235409.
(42) Puzder, A.; Williamson, A. J.; Gygi, F.; Galli, G. *Phys. Rev. Lett.* **2004**, *92*, 217401.
(43) del Puerto, M.; Tiago, M.; Chelikowsky, J. *Phys. Rev. Lett.* **2006**, *97*, 1.
(44) Yu, M.; Fernando, G. W.; Li, R.; Papadimitrakopoulos, F.; Shi, N.; Ramprasad, R. *Appl. Phys. Lett.* **2006**, *88*, 231910.
(45) Botti, S.; Marques, M. *Phys. Rev. B* **2007**, *75*, 1.
(46) Kilina, S.; Ivanov, S.; Tretiak, S. *J. Am. Chem. Soc.* **2009**, *131*, 7717.
(47) Spanó, E.; Hamad, S.; Catlow, C. R. a. *J. Phys. Chem. B* **2003**, *107*, 10337.
(48) Hamad, S.; Catlow, C. R. A.; Spanò, E.; Matxain, J. M.; Ugalde, J. M. *J. Phys. Chem. B* **2005**, *109*, 2703.
(49) Hamad, S.; Catlow, R. A. *J. Cryst. Growth* **2006**, *294*, 2.
(50) Huang, T. T.; Tan, K.; Lin, M. H. *J. Mol. Struct. (THEOCHEM)* **2007**, *821*, 101.
(51) Chen, H.; Shi, D.; Qi, J.; Jia, J.; Wang, B. *Phys. Lett. A* **2009**, *373*, 371.
(52) Gu, Y.; Tan, K.; Lin, M. *J. Mol. Struct. (THEOCHEM)* **2010**, *961*, 62.
(53) Zhang, D.; Chen, L.; Zhang, J.; Miao, X. *J. Am. Ceram. Soc.* **2011**, *94*, 759.
(54) Zhang, X.; Zhao, M.; He, T.; Li, W.; Lin, X.; Wang, Z.; Xi, Z.; Liu, X.; Xia, Y. *Solid State Commun.* **2008**, *147*, 165.
(55) Zhang, X.; Zhao, M.; Yan, S.; He, T.; Li, W.; Lin, X.; Xi, Z.; Wang, Z.; Liu, X.; Xia, Y. *Nanotechnology* **2008**, 305708.
(56) Azpiroz, J. M.; Mosconi, E.; Angelis, F. D. *J. Phys. Chem. C* **2011**, *115*, 25219−.
(57) Zwijnenburg, M. A.; Sousa, C.; Illas, F.; Bromley, S. T. *J. Chem. Phys.* **2011**, *134*, 064511-1.
(58) Azpiroz, J. M.; Infante, I.; Lopez, X.; Ugalde, J. M.; De Angelis, F. *J. Mater. Chem.* **2012**, *22*, 21453.
(59) Azpiroz, J. M.; Lopez, X.; Ugalde, J. M.; Infante, I. *J. Phys. Chem. C* **2012**, *116*, 2740.
(60) Liu, C.; Chung, S. Y.; Lee, S.; Weiss, S.; Neuhauser, D. *J. Chem. Phys.* **2009**, *131*, 174705.
(61) Vilhena, J. G.; Botti, S.; Marques, M. a. L. *Appl. Phys. Lett.* **2010**, *96*, 123106.
(62) Voznyy, O. *J. Phys. Chem. C* **2011**, *115*, 15927.
(63) Lee, J. R. I.; Whitley, H. D.; Meulenberg, R. W.; Wolcott, A.; Zhang, J. Z.; Prendergast, D.; Lovingood, D. D.; Strouse, G. F.; Ogitsu, T.; Schwegler, E.; Terminello, L. J.; van Buuren, T. *Nano Lett.* **2012**, *12*, 2763.
(64) Bhattacharya, S. K.; Kshirsagar, A. *Eur. Phys. J. D* **2008**, *48*, 355.
(65) Azpiroz, J. M.; Matxain, J. M.; Infante, I.; Lopez, X.; Ugalde, J. M. *Phys. Chem. Chem. Phys.* **2013**, *15*, 10996.
(66) Del Ben, M.; Havenith, R. W. A.; Broer, R.; Stener, M. *J. Phys. Chem. C* **2011**, *115*, 16782.
(67) Kilin, D. S.; Tsemekhman, K.; Prezhdo, O. V.; Zenkevich, E. I.; von Borczyskowski, C. *J. Photochem. Photobiol., A* **2007**, *190*, 342.
(68) Zhang, X.; Zhang, H.; He, T.; Zhao, M. *J. Appl. Phys.* **2010**, *108*, 064317.
(69) Krainara, N.; Limtrakul, J.; Illas, F.; Bromley, S. *Phys. Rev. B* **2011**, *83*, 1.
(70) Sangthong, W.; Limtrakul, J.; Illas, F.; Bromley, S. T. *Nanoscale* **2010**, *2*, 72.
(71) Kilina, S. V.; Kilin, D. S.; Prezhdo, O. V. *ACS Nano* **2009**, *3*, 93.
(72) Deglmann, P.; Ahlrichs, R.; Tsereteli, K. *J. Chem. Phys.* **2002**, *116*, 1585.
(73) Malloci, G.; Chiodo, L.; Rubio, A.; Mattoni, A. *J. Phys. Chem.C* **2012**, *116*, 8741.
(74) Zwijnenburg, M. A. *Nanoscale* **2011**, *3*, 3780.
(75) Zwijnenburg, M. A. *Nanoscale* **2012**, *4*, 3711.
(76) Nguyen, K. A.; Day, P. N.; Pachter, R. *J. Phys. Chem. C* **2010**, *114*, 16197.
(77) Matxain, J. M.; Fowler, J. E.; Ugalde, J. M. *Phys. Rev. A* **2000**, *61*, 53201.
(78) Wang, C.; Xu, S.; Ye, L.; Lei, W.; Cui, Y. *Struct. Chem.* **2010**, *21*, 1215.
(79) Zwijnenburg, M. A.; Illas, F.; Bromley, S. T. *Phys. Chem. Chem. Phys.* **2011**, *13*, 9311.
(80) Matxain, J.; Mercero, J.; Fowler, J.; Ugalde, J. *Phys. Rev. A* **2001**, *64*, 1.
(81) Mohajeri, A.; Alipour, M. *Int. J. Quantum Chem.* **2011**, *111*, 3888.
(82) Xu, S.; Wang, C.; Cui, Y. *Int. J. Quantum Chem.* **2011**, *111*, 156.
(83) Chung, S.-Y.; Lee, S.; Liu, C.; Neuhauser, D. *J. Phys. Chem. B* **2009**, *113*, 292.
(84) Inerbaev, T. M.; Masunov, A. E.; Khondaker, S. I.; Dobrinescu, A.; Plamadă, A.-V.; Kawazoe, Y. *J. Chem. Phys.* **2009**, *131*, 044106.
(85) Kim, H.-S.; Jang, S.-W.; Chung, S.-Y.; Lee, S.; Lee, Y.; Kim, B.; Liu, C.; Neuhauser, D. *J. Phys. Chem. B* **2010**, *114*, 471.
(86) Xu, S.; Wang, C.; Cui, Y. *J. Mol. Model.* **2010**, *16*, 469.
(87) Yang, P.; Tretiak, S.; Ivanov, S. *J. Cluster Sci.* **2011**, *22*, 405.
(88) Koposov, A. Y.; Cardolaccia, T.; Albert, V.; Badaeva, E.; Kilina, S.; Meyer, T. J.; Tretiak, S.; Sykora, M. *Langmuir* **2011**, *27*, 8377.
(89) Fischer, S. a.; Crotty, A. M.; Kilina, S. V.; Ivanov, S. a.; Tretiak, S. *Nanoscale* **2012**, *4*, 904.
(90) Kuznetsov, A. E.; Balamurugan, D.; Skourtis, S. S.; Beratan, D. N. *J. Phys. Chem. C* **2012**, *116*, 6817.
(91) Lim, E.; Kuznetsov, A. E.; Beratan, D. N. *Chem. Phys.* **2012**, *407*, 97.
(92) Xu, S.; Wang, C.; Cui, Y. *Struct. Chem.* **2010**, *21*, 519.
(93) Matxain, J. M.; Irigoras, A.; Fowler, J. E.; Ugalde, J. M. *Phys. Rev. A* **2001**, *64*, 13201.
(94) Matxain, J. M.; Eriksson, L. a.; Mercero, J. M.; Ugalde, J. M.; Spano, E.; Hamad, S.; Catlow, C. R. a. *Nanotechnology* **2006**, *17*, 4100.
(95) Kasuya, A.; Sivamohan, R.; Barnakov, Y. a.; Dmitruk, I. M.; Nirasawa, T.; Romanyuk, V. R.; Kumar, V.; Mamykin, S. V.; Tohji, K.; Jeyadevan, B.; Shinoda, K.; Kudo, T.; Terasaki, O.; Liu, Z.; Belosludov, R. V.; Sundararajan, V.; Kawazoe, Y. *Nat. Mater.* **2004**, *3*, 99.

(96) Becke, A. D. *Phys. Rev. A* **1988**, *38*, 3098.
(97) Lee, C.; Yang, W.; Parr, R. G. *Phys. Rev. B* **1988**, *37*, 785.
(98) Hay, P. J.; Wadt, W. R. *J. Chem. Phys.* **1985**, *82*, 299.
(99) Hay, P. J.; Willard, R. W. *J. Chem. Phys.* **1985**, *82*, 270.
(100) Wadt, W. R.; Hay, P. J. *J. Chem. Phys.* **1985**, *82*, 284.
(101) Perdew, J. P. *Phys. Rev. B* **1986**, *33*, 8822.
(102) Binkley, J. S.; Pople, J. A.; Hehre, W. J. *J. Am. Chem. Soc.* **1979**, *102*, 939.
(103) Cundari, T. R.; Steven, W. J. *J. Chem. Phys.* **1993**, *98*, 5555.
(104) Stevens, W. J.; Krauss, M.; Basch, H.; Jasien, P. P. G. *Can. J. Chem.* **1992**, *70*, 612.
(105) Perdew, J. P.; Chevary, J. A.; Vosko, S. H.; Jackson, K. A.; Pederson, M. R.; Singh, D. J.; Fiolhais, C. *Phys. Rev. B* **1992**, *46*, 6671.
(106) Weigend, F.; Ahlrichs, R. *Phys. Chem. Chem. Phys.* **2005**, *7*, 3297.
(107) Andrade, D.; Häubermann, U.; Dolg, M.; Stoll, H.; Preub, H. *Theor. Chim. Acta* **1990**, *77*, 123.
(108) Adamo, C.; Barone, V. *J. Comput. Chem.* **1998**, *19*, 418.
(109) Gill, P. M. W. *Mol. Phys.* **1996**, *89*, 433.
(110) Adamo, C.; Barone, V. *J. Chem. Phys.* **1998**, *108*, 664.
(111) Lenthe, E. V.; Baerends, E. J. *J. Comput. Chem.* **2003**, *24*, 1142.
(112) Handy, N. C.; Cohen, A. J. *Mol. Phys.* **2001**, *99*, 403.
(113) Hoe, W.-M.; Cohen, A.; Handy, N. C. *Chem. Phys. Lett.* **2001**, *341*, 319.
(114) Perdew, J. P.; Burke, K.; Ernzerhof, M. *Phys. Rev. Lett.* **1996**, *77*, 3865.
(115) Adamo, C.; Barone, V. *Chem. Phys. Lett.* **1997**, *274*, 242.
(116) Becke, A. D. *J. Chem. Phys.* **1993**, *98*, 5648.
(117) Wilson, P. J.; Bradley, T. J.; Tozer, D. J. *J. Chem. Phys.* **2001**, *115*, 9233.
(118) Cohen, A. J.; Handy, N. C. *Mol. Phys.* **2001**, *99*, 607.
(119) Adamo, C.; Barone, V. *J. Chem. Phys.* **1999**, *110*, 6158.
(120) Xu, X.; Goddard, W. A., III. *Proc. Natl. Acad. Sci. U. S. A.* **2004**, *101*, 2673.
(121) Grimme, S. *J. Comput. Chem.* **2006**, *27*, 1787.
(122) Boese, A. D.; Doltsinis, N. L.; Handy, N. C.; Sprik, M. *J. Chem. Phys.* **2000**, *112*, 1670.
(123) Boese, A. D.; Handy, N. C. *J. Chem. Phys.* **2001**, *114*, 5497.
(124) Hamprecht, F. A.; Cohen, A.; Tozer, D. J.; Handy, N. C. *J. Chem. Phys.* **1998**, *109*, 6264.
(125) Zhao, Y.; Truhlar, D. G. *J. Chem. Phys.* **2006**, *125*, 194101-1.
(126) Zhao, Y.; Schultz, N. E.; Truhlar, D. G. *J. Chem. Phys.* **2005**, *123*, 161103-1.
(127) Zhao, Y.; Schultz, N. E.; Truhlar, D. G. *J. Chem. Theory Comput.* **2006**, *2*, 364.
(128) Zhao, Y.; Truhlar, D. G. *Theor. Chem. Acc.* **2008**, *120*, 215.
(129) Zhao, Y.; Truhlar, D. G. *J. Phys. Chem. A* **2006**, *110*, 5121.
(130) Zhao, Y.; Truhlar, D. G. *J. Phys. Chem. A* **2006**, *110*, 13126.
(131) Tao, J. M.; Perdew, J. P.; Staroverov, V. N.; Scuseria, G. E. *Phys. Rev. Lett.* **2003**, *91*, 146401-1.
(132) Yanai, T.; Tew, D.; Handy, N. *Chem. Phys. Lett.* **2004**, *393*, 51.
(133) Vydrov, O. A.; Heyd, J.; Krukau, A.; Scuseria, G. E. *J. Chem. Phys.* **2006**, *125*, 074106-1.
(134) Vydrov, O. A.; Scuseria, G. E. *J. Chem. Phys.* **2006**, *125*, 234109-1.
(135) Vydrov, O. A.; Scuseria, G. E.; Perdew, J. P. *J. Chem. Phys.* **2007**, *126*, 154109-1.
(136) Chai, J.-D.; Head-Gordon, M. *Phys. Chem. Chem. Phys.* **2008**, *10*, 6615.
(137) Wu, S.; Liu, H.; Liu, H.; Wu, Z.; Du, Z.; Schelly, Z. A. *Nanotechnology* **2007**, *18*, 485607-1.